Chapter 11

Teleconnections between tropical SST modes and Indian summer monsoon in observation and CMIP5 models

Indrani Roy[a], **Ramesh Kripalani**[b]
[a]*University College London (UCL), IRDR, London, United Kingdom,* [b]*Indian Institute of Tropical Meteorology (MoES), Pune, India (retired)*

11.1 Introduction

The Indian summer monsoon (ISM) plays a critical role in the well-being of a billion people. ISM serves a very important part of India's socioeconomic infrastructure as it receives about 80% of the total rainfall during this season. Society is so finely tuned to its rains that its variation has profound impacts on country's industry, agriculture, and economy. As India has the second largest population in the world, it also has consequences for global wealth generation. Variability of ISM is strongly influenced by sea surface temperature (SST) of tropics, among which El Niño Southern Oscillation (ENSO) and the Indian Ocean Dipole (IOD) are two dominant modes of climate variability.

ENSO, the most dominant tropospheric variability around tropical Pacific is found to be strongly coupled with the ISM (Azad and Rajeevan, 2016; Kumar, 2006; Ashok, 2001; Roy, 2018a; Li et al., 2017; Hrudya et al., 2020b; Sikka, 1980; Rasmussen and Carpenter, 1983). Excess rainfall years in India are usually aligned with cold events of ENSO or La Niña years, while drought years match with El Niño. SST anomaly in the Pacific in opposite phases of ENSO are shown in Fig. 11.1A. Studies also detected some complementary effects of the IOD on ISM (Ashok et al., 2001). However, such linkages were shown could be sensitive to the reference period chosen (Roy and Collins, 2015; Roy, 2018b).

In the tropical Indian Ocean (IO), one of the leading modes of interannual variability is the IOD. IOD index is measured by the difference in SST anomaly between the western equatorial IO and the south eastern equatorial IO. It has a profound impact on the climate and weather of India, Australia, and East Africa.

Indian Summer Monsoon Variability: El Niño-teleconnections and beyond.
DOI: https://doi.org/10.1016/B978-0-12-822402-1.00012-0

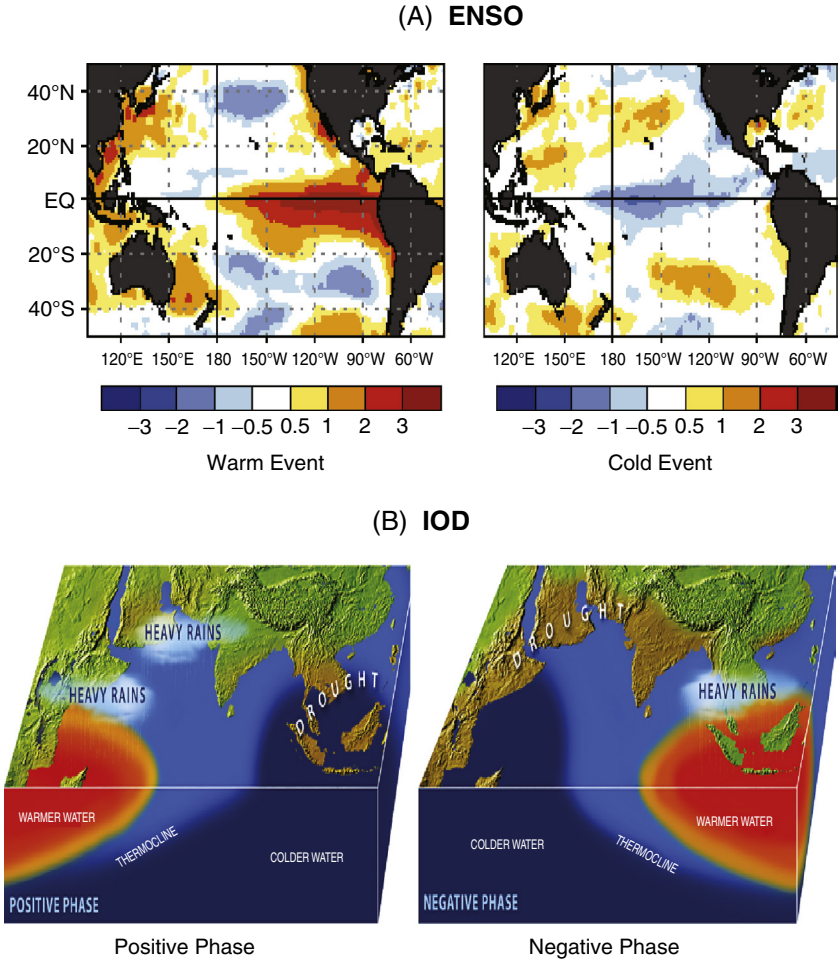

FIG. 11.1 Opposite phases of the (A) ENSO showing reverse sea surface temperature anomaly in the tropical Pacific [http://www.cpc.noaa.gov/products/analysis_ monitoring/ ensocycle/] and (B) Indian Ocean Dipole and effects [http://www.whoi.edu/] (Accessed 31 December 2020). "*ENSO*, El Niño southern oscillation."

Different characteristics of IOD and its impact are discussed elaborately in various studies (Saji et al. 1999, 2003; Webster et al., 1999; Hrudya et al., 2020b). During the negative phase of IOD, SST is anomalously cold in the western equatorial region of IO, while warm in the eastern side and the reverse is true for the positive phase (Fig. 11.1B). During the positive (negative) phase of the IOD, Darwin in Australia experiences drought (heavy rain) which is also associated with cold (warm) surrounding ocean water. On the other hand, in India or East Africa, there is heavy rainfall in the positive IOD phase and less rainfall in the negative phase. The impact of IOD is mainly seen around countries

adjacent to the IO; whereas, ENSO though originated in the tropical Pacific Ocean, have profound impacts in most parts of the globe (Brown et al., 2009; Cai et al., 2009; Roy, 2018a; Tedeschi and Collins, 2016; Preethi et al., 2015). It has become common to discuss two types of ENSO. One is dominated by the variability of SST centered in the Eastern Tropical Pacific, commonly known as the East Pacific (EP) type or Canonical ENSO, and the other dominated by strong SST variability around the central tropical Pacific, commonly known as Central Pacific (CP) type or ENSO Modoki (Ashok et al., 2007; Kao et al., 2009; Kug et al., 2009).

The teleconnection patterns associated with these two ENSO types indicate different impacts on various parts of the world (Australia: Cai and Cowan, 2009; Brown et al., 2009; South America: Tedeschi and Collins, 2016; Tedeschi et al., 2013; India: Ashok et al., 2007; Roy et al., 2017; Roy et al., 2019). The formation mechanisms of these two ENSO types are also different; for the Canonical case, the thermocline plays a dominant role, while for Modoki, zonal advection and mid-latitude interactions are proposed as more important (Kao et al. 2009; Yu et al. 2011). Different solar decadal influence on the mechanisms of these two types of ENSO is also recently explored (Roy and Kripalani, 2019a).

Another new type of ENSO named the "mega-ENSO," has been identified (Wang et al., 2013; Zhang et al., 2017 and Wu and Zhang, 2015). It has a pattern similar to the interdecadal Pacific oscillation but involves both interannual and multidecadal SST variations. Many researchers also discussed other types of ENSO events and their impact on ISM. For example, Zhang et al. (2016) analyzed different impacts of atypical and typical developing ENSOs on the ISM. The current study, however, focuses mainly on Canonical and Modoki types of ENSO.

Various modeling groups around the world have coordinated climate model experiments, known as Coupled Model Intercomparison Project (CMIP5) (Taylor et al. 2012). Experiments with various radiative forcing scenarios were also examined in hypothetical future climate change situations (Riahi et al. 2011). Representative Concentration Pathways 8.5 (RCP 8.5) scenarios are the highest forcing situations as examined. These model simulations may be used to better understand the ENSO–ISM teleconnection during various types of ENSO events and changes under climate change (Li et al., 2017; Jourdain et al., 2013; Roy and Tedeschi, 2016; Roy et al., 2017; Roy et al., 2019; Azad and Rajeevan, 2016).

The ISM represents a large-scale heat source along the equator around the intertropical convergence zone that covers Central North East (CNE) India. Following the linear theory, it is linked to both the regional Hadley cell as well as the Walker Circulation (Gill, 1980), and hence the main focus of many recent analyses was on the CNE region (Roy et al. 2017; Bollasina et al. 2011; Goswami et al. 2006). Earlier works studied extratropical ENSO teleconnections in CMIP5 models (Hurwitz et al., 2014; Charlton-Perez, 2013) separating models as the high top (H) and low top (L). H models have upper lids up to the Stratopause (1 hPa) and it is believed that these models with polar vortex

features may capture polar annular mode patterns better (Osprey et al., 2013; Seviour et al., 2016; Charlton-Perez, 2013). ISM—southern annular mode teleconnection in observations was also identified, where ENSO Modoki plays the dominant part (Prabhu et al., 2016). Studies further separated CMIP5 models based on H or L to detect whether it is possible to segregate a subset of models performing better over the others (Roy et al., 2017, 2019).

Changes of ISM in the future had been analyzed (Azad and Rajeevan, 2016; Zou and Zhou, 2015; Roy, 2017) that suggested a significant change from the historical period. Azad and Rajeevan (2016) used 20 different CMIP5 models and studied ISM and ENSO teleconnection in a future scenario and suggested a shift to a shorter period from 2.5 to 3 years in the future from 3- to 5-year period band of variability of the historical period. How ISM–ENSO teleconnection will evolve in the future, especially when the focus is on the various subcategories of ENSO were also explored in recent studies (Roy et al. 2019).

Various thermodynamic scaling arguments had been put forward to explain future changes in ISM (Held and Soden, 2006). Those included "wet get wetter" (Chou et al., 2009) and "warmer-get-wetter" (Xie et al., 2010; John et al., 2009) concept. Recent studies suggest that changes in circulation are crucial (Seager et al., 2010) and hence it is appropriate to use techniques to decompose ISM rainfall changes associated with both circulation and moisture. Studies (Roy et al., 2019) employed such a technique to explain the changes in ISM rainfall under climate change considering the effect of both "thermodynamical" and "dynamical" part (Chung et al., 2014; Seager et al., 2012). It discussed changes in the behavior of ENSO–ISM teleconnection during differently flavored ENSO situations (Huang and Xie, 2015; Huang, 2014).

As ENSO plays a crucial role in the variation of ISM, improved understanding of ENSO could be a step forward on advanced ISM prediction. The work of Cappondonti et al. (2015) nicely discussed the current state of understanding on ENSO diversity and identified major areas of knowledge gaps. Studies pointed out that more attention is needed on the tropical/extratropical teleconnections associated with ENSO (Roy et al. 2018). It discussed that bias correction in models could be an important area of model improvements and highlighted the strengths and weaknesses of CMIP5 models in different oceanic sectors that not only included Pacific but also Atlantic. The link between changes in ENSO and the mean state of the Pacific climate would be an important area that needs to be explored to understand the varied nature of ENSO in the future (Cai et al. 2015). Interestingly, Yeh et al. (2018) discussed that future changes of ENSO teleconnection do not currently indicate strong agreement among models.

Disruption of ISM–ENSO teleconnection in later decades was discussed (Hrudya et al., 2020a; Seetha et al., 2020; Kripalani and Kulkarni, 1997; Krishna Kumar et al., 1999) with particular emphasis on the latter two decades of the 20th century (Roy, 2018b; Roy and Kripalani, 2019a, 2019b). Most models are unable to reproduce this observed change in the ENSO–monsoon relationship. Instead the models have a strong inverse relationship between monsoon and

ENSO, similar to the observations in the earlier period (Preethi et al., 2010; Rajeevan et al., 2012). Those studies have also shown that the large bias in SST over the IO and the imperfect relationship of monsoon with ENSO and IOD are some of the possible reasons for the lower skill of the models in simulating monsoons during the recent period, compared to the previous period. Other studies further indicated that Pacific Ocean, as well as North Atlantic, also played roles in the change in the pattern of ISM teleconnection (Roy, 2020, 2018b). The role of natural factors was addressed which suggested that the mean state of the Pacific climate and regions of the North Atlantic served crucial parts. CMIP5 model results, in these connections, were shown poorly representing observed influences of natural factors (Roy, 2018b; Roy and Kripalani, 2019b). A hypothesized mechanism is proposed for such a disruption in ISM– ENSO teleconnection which indicated that regional Hadley circulation played a major role (Roy, 2018b).

Overall, this chapter presents a brief overview of our general understanding of teleconnections between some important tropical SST modes and ISM in observation and CMIP5 models. It further indicates areas of biases in CMIP5 models and provides directions for reducing uncertainties in simulating ISM.

11.2 Tropical ocean SST teleconnections to ISM

11.2.1 ISM-IOD teleconnection: Observations

IOD develops in boreal summer (JJA) while peaks in fall (SON) (Saji et al., 1999; Webster et al., 1999). In recent decades two extreme positive IOD occurred, one during 1997 and the other in 2019. During 1997, extreme IOD resulted in drought and bushfire in Indonesia and Australia, whereas flooding in the Eastern part of Africa (Saji et al., 1999; Webster et al., 1999). Another extreme IOD happened in 2019 and it is believed that it has a relevance to widespread Australian bush fire during that year. ISM in 2019, June through September was an excess monsoon (110% of long-period average), whereas the previous excess monsoon was during 1994. There is a positive skewness of the IOD, where positive events tend to be stronger in amplitude than negative events (Cai et al., 2012; Ogata et al., 2012). Australia's millennium drought may be explained in light of tendencies of IOD events (Ummenhofer et al., 2009). Not only IOD, but IOD-ENSO combined behavior is also important and can influence regional rainfall patterns (see Chapter 8). Teleconnections of ENSO, ENSO Modoki, and IOD with rainfall over different parts of the world, especially the East African rainfall was discussed by Preethi et al. (2015). It also showed opposite impacts during some seasons. ENSO and IOD exert an offsetting impact on ISM, with El Niño tend to lower ISM rainfall, whereas a positive IOD tends to increase that (Hrudya et al., 2020b; Li et al., 2017; Ashok et al., 2004).

Using reanalysis and model, correspondence between ENSO, IOD, and ISM was studied in detail (Cherchi and Navarra, 2013; Behera et al., 2006; Krishnaswamy et al., 2014). Fig. 11.2 represents a schematic depicting the

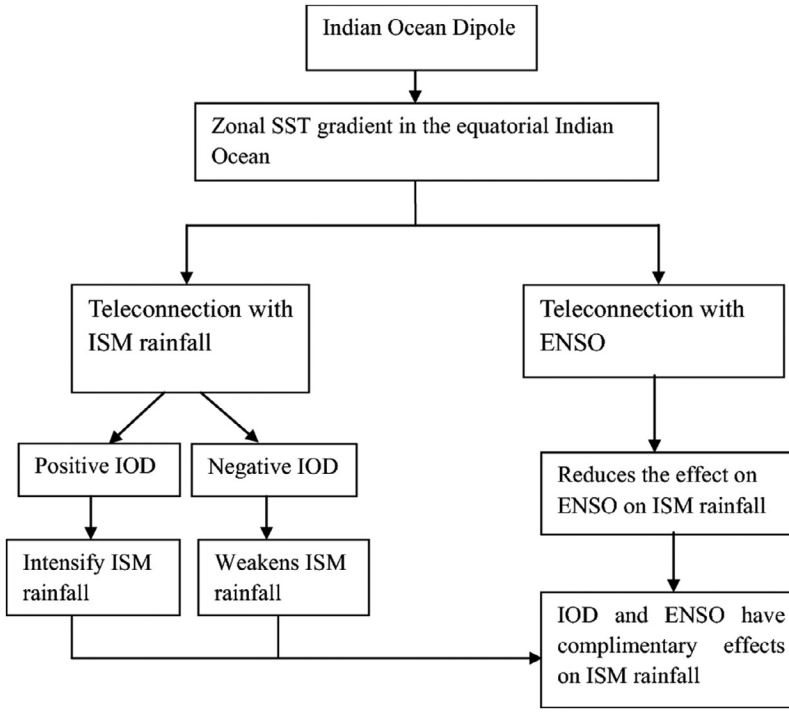

FIG. 11.2 A schematic showing the IOD–ENSO and IOD–ISM relationships (Hrudya et al., 2020b). "*ENSO*, El Niño southern oscillation; *IOD*, Indian Ocean Dipole; *ISM*, Indian summer monsoon."

observed IOD–ENSO and IOD–ISM relationships. Variability in the tropical IO has also found to be strongly connected with the phase of both ENSO and IOD (Chakravorty et al. 2013). Studies also suggested that decadal variability in tropical IO SST influences the monsoon dynamics, that involve Hadley and Walker circulation and modulates ISM (Vibhute et al., 2020; Roy and Collins, 2015). From the observed record, ENSO–IOD correlation is found positive and significant since later decades of the 20th century which may correspond with either weak/strong monsoon–ENSO relationship or strong/weak monsoon–IOD relationship (Cherchi and Navarra, 2013). It is consistent with the fact that over the same time, the teleconnection between ISM–ENSO weakened (Kripalani and Kulkarni, 1997; Krishna Kumar et al., 1999), whereas the relationship strengthened for ISM–IOD (Ashok et al. 2001).

In Table 11.1, IOD years are computed from values averaged in SON exceeding 1 standard deviation (std) from the mean (see details in Cherchi and Navarra, 2013). Those mostly agree with previous classifications (Yuan and Yin, 2008; Saji and Yamagata, 2003, among others). ENSO years are based on November-December-January values exceeding 0.5 std. All La Niña/El

TABLE 11.1 List of La Niña, El Niño, negative, and positive Indian Ocean Dipole years.

	List of years
El Niño	1951 **1957**, 1963, **1965**, 1968, 1969, **1972**, 1976, 1977, **1982**, 1986, 1987, **1991**, **1994**, **1997**, 2002
La Niña	**1949**, 1950, 1954, **1955**, 1956, 1964, 1967, **1970**, 1971, **1973**, **1975**, **1984**, **1988**, 1995, 1998, **1999**, 2000
positive IOD	1961, 1963, 1967, 1972, 1982, 1987, 1991, 1994, 1997, 2002
negative IOD	1956, 1958, 1960, 1964, 1968, 1974, 1975, 1992, 1996, 1998

Cherchi and Navarra (2013)

Niño years in the table agree with the US National Weather Service classification (http://www.cdc.noaa.gov/products/analysis_monitoring/ensostuff/ensoyears.html). Years exceeding 1 std are in bold. At least half the time potentially predictable monsoon years coincide with a positive IOD event or an El Niño (Cherchi and Navarra, 2013). In fact, for all the cases the two events co-occurred; whereas, the correspondence is weaker for negative IOD and La Niña events.

11.2.2 ISM–IOD teleconnection: model results

Community Earth System Model Large Ensemble (CESM-LE) and CMIP5 models simulated well the seasonal phase-locking of IOD (Liu et al., 2014; Hui et al., 2018). A modeling study conducted IODs response under increased greenhouse gas scenario and found models have limitations to account for the role of internal climate variability (Ng et al., 2018). A small difference in the depth of mean thermocline, which is caused by internal climate variability, generates significant variations in the skewness, amplitude of IOD, and the climatological zonal SST gradient. They used the simulations from the CESM-LE model for present-day cases as well as for the future. The performance of 21 CMIP5 models in the simulation of IOD is evaluated and compared with the CMIP3 version (Liu et al. 2014). It is noticed that the ENSO and IOD amplitudes are closely related in models, e.g., if a model generates a weak/strong ENSO, it is likely to simulate a weak/strong IOD too.

Analyzing 34 CMIP5 models, IOD, ENSO, and ISM were analyzed in both historical and future scenarios (Li et al. 2017). For observation, they considered the period 1950–1999. Due to an overly strong control by ENSO, the majority of models simulate an unrealistic IOD and ISM rainfall (ISMR) correlation (Fig. 11.3). In the simulated present-day scenario, a positive IOD is associated with a reduction in ISM rainfall (Fig. 11.3C), which is different from what we discussed in Figs 11.1B and 11.2. Models with a larger IOD amplitude produce a greater ISM–IOD negative correlation. Such an unrealistic

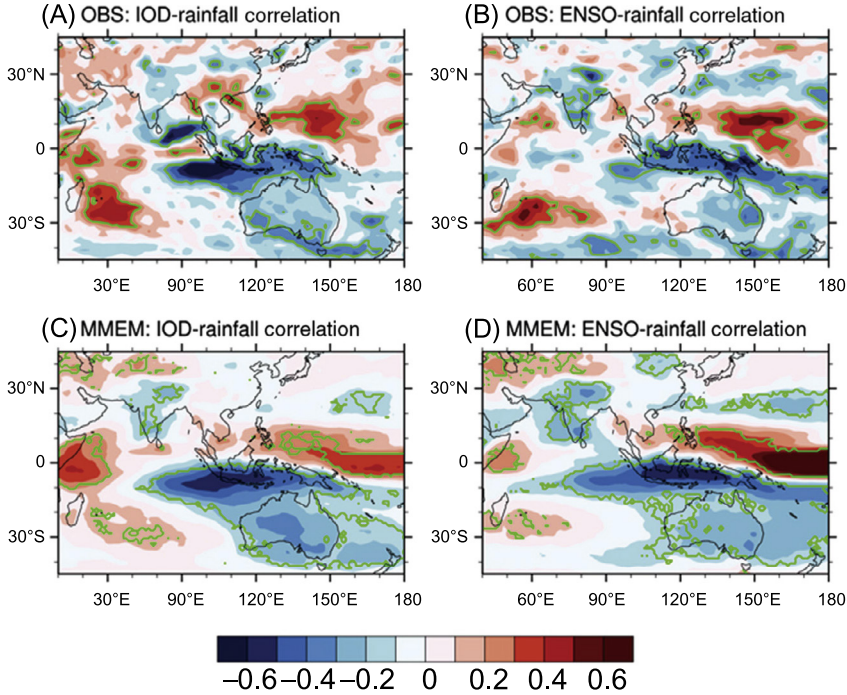

FIG. 11.3 Present-day rainfall correlations with IOD (left) and ENSO (right) for observation (top, A and B) and using the multimodel ensemble mean (MMEM) (bottom, C and D). In (A) and (B) areas within the green contours indicate regions where the correlation is statistically significant above the 95% level. In (C) and (D) the green contours show areas where the sign of the correlation is consistent over 80% of CMIP5 models (Li et al., 2017). "*ENSO*, El Niño southern oscillation; *IOD*, Indian Ocean Dipole."

correlation of the historical period is relevant to the future projection of ISM and will induce an underestimation/overestimation in the projected rainfall. The impact on ISMR from the ENSO and IOD tends to offset and was seen in model simulations as well as in observations. For example, the El Niño of 1997 was strongest in the last century, which alone would reduce ISMR. However, the influence of ENSO on ISMR was overwhelmed by the concurrent 1997 extreme positive IOD event, which was liable for a moderate increase in ISMR. There is no significant rainfall response to IOD events seen in Fig. 11.3A, as the dominant and concurrent effect from ENSO suppresses the impact from IOD. Positive correlation in observation for IOD is only noticed around north eastern region of India. Rainfall responses to ENSO, however, indicates a broadly consistent and significant region, i.e., a reduction in ISM rainfall during El Niño and vice versa for La Niña. (Fig. 11.3B). Uncertainties in the projection of ISM can partly be induced by present-day simulation of ENSO, IOD, their connection and correlations with ISM

(Li et al. 2017). However, there is some consistency around CNE region for either rainfall ENSO teleconnection or rainfall IOD teleconnection through the sign for IOD is different (Fig. 11.3).

11.2.3 ISM–ENSO teleconnection

Similar to IOD, ENSO also develops in boreal summer (JJA) though peaks in boreal winter (DJF) (Wang and Fiedler, 2006). Jourdain et al. (2013) discussed spatial pattern of ISM rainfall using CMIP5 (Fig. 11.4) and CMIP3 models and addressed ISM ENSO teleconnection. Climatological spatial pattern suggests that there are more rainfall in parts of Eastern India and also along regions of Western Ghat from South India. It is followed by the CNE region, which also receives high rainfall. Some CMIP5 models capture such spatial patterns reasonably well and those model results with their names (total 9 in number) and are shown in Fig. 11.4 (right). Recent studies, however, indicated that there is disagreement among models in various ISM-related features (Roy, 2017). For example, in the CNE region of India, a decreasing trend is noticed for ISM in observation during the latter decades of the last century (Bollasina et al., 2011; Goswami et al., 2006) and in one chosen model NOAA GFDL CM3 (Bollasina et al. 2011, shown in Fig. 11.5). That is one feature of ISM among others that suggests inconsistency among CMIP5 models (Roy, 2017). Regions from CNE as used by Bollasina et al. (2011) and Goswami et al. (2006) are marked by CI (76°–87°E, 20°–28°N) and CII (74.5°E–86.5°E and 16.5°N–26.5°N), respectively, in Fig. 11.6. Precipitation time series around the Indian subcontinent vary widely among models and analyses with various future scenarios indicate that the Indian subcontinent shows much larger uncertainty, compared to that from the whole world (Roy, 2017).

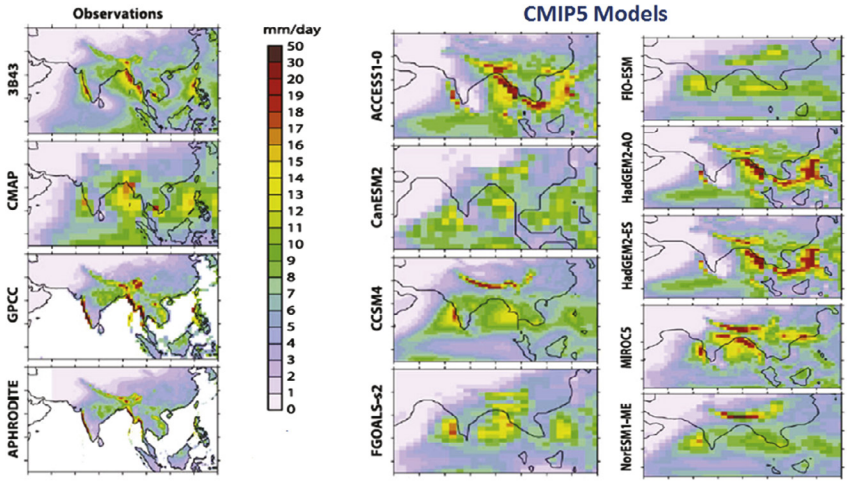

FIG. 11.4 Rainfall climatology in various observations (left) and in historical CMIP5 simulations (right) (after, Jourdain et al. 2013).

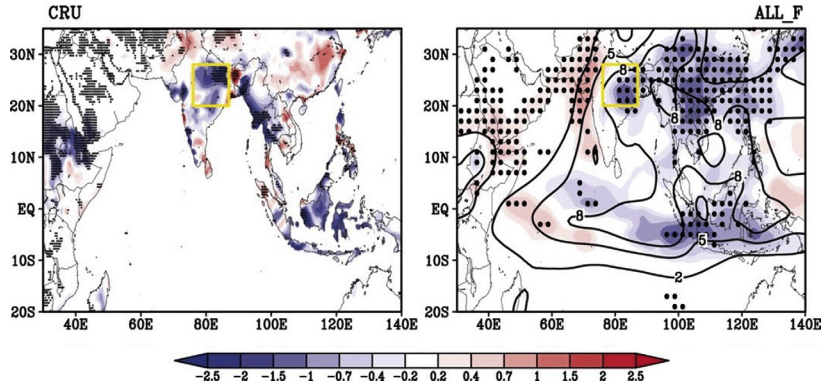

FIG. 11.5 A decreasing trend of ISM rainfall in CNE region of India in observation (CRU data) shown left and the model NOAA GFDL CM3 using all forcing (natural and anthropogenic) shown right (Bollasina et al., 2011). "*CNE*, Central North East*; ISM*, Indian summer monsoon."

11.2.4 ISM in various ENSO phases: historical period

To address various ENSO phases, different locations of the Pacific Ocean need to be identified. Those regions can be marked (Fig. 11.6A) as follows: Canonical region (5°N–5°S, 90°W–140°W), region A (10°S–10°N, 165°E–140°W), region B (15°S–5°N, 110°W–70°W) and region C (10°S–20°N, 125°E–145°E).

Following SST anomalies (SSTAs) in those regions, various definitions for ENSO are used (Ashok et al., 2007; Kao et al., 2009; Kug et al., 2009; Tedeschi et al., 2013):

- ENSO Modoki Index (EMI).
  EMI = (region A SSTA) – 0.5(region B SSTA) – 0.5(region C SSTA).
- ENSO Modoki (ENM/LNM): EMI is greater/less than $0.7\sigma_M$ and region A SSTA is greater than $0.7\sigma_A$. σ_M is the standard deviation (std) of the EMI and σ_A is the std of the region A SSTAs.
- ENSO Canonical (ENC/LNC): SSTA in the Canonical region is greater/less than $0.7\sigma_C$, σ_C is std of SSTAs in that region.
- Mixed ENSO Canonical and Modoki (ENCM/LNCM): SSTAs satisfy both the Canonical as well as Modoki conditions.

Recent studies discussed ISM–ENSO teleconnection in various ENSO phases (Roy et al., 2017, 2019; Roy and Tedeschi, 2016). Correlation and compositing techniques (Ashok et al., 2007; Tedeschi et al., 2013) were mainly used, while the trend was initially removed from the data. Regional teleconnection in specified locations of India (as shown in Fig. 11.6B and C) was also addressed. For correlation analyses, correlation between ISM rainfalls with the SST of canonical region, region A and the EMI index were computed and respective spatial plots were analyzed. The level of significance for the correlation analysis was tested using Student's *t* test. For compositing, the average value of various meteorological parameters (precipitation, meridional, and zonal wind at 850 mb and 200 mb) was calculated for chosen Indian regions, in various ENSO phases.

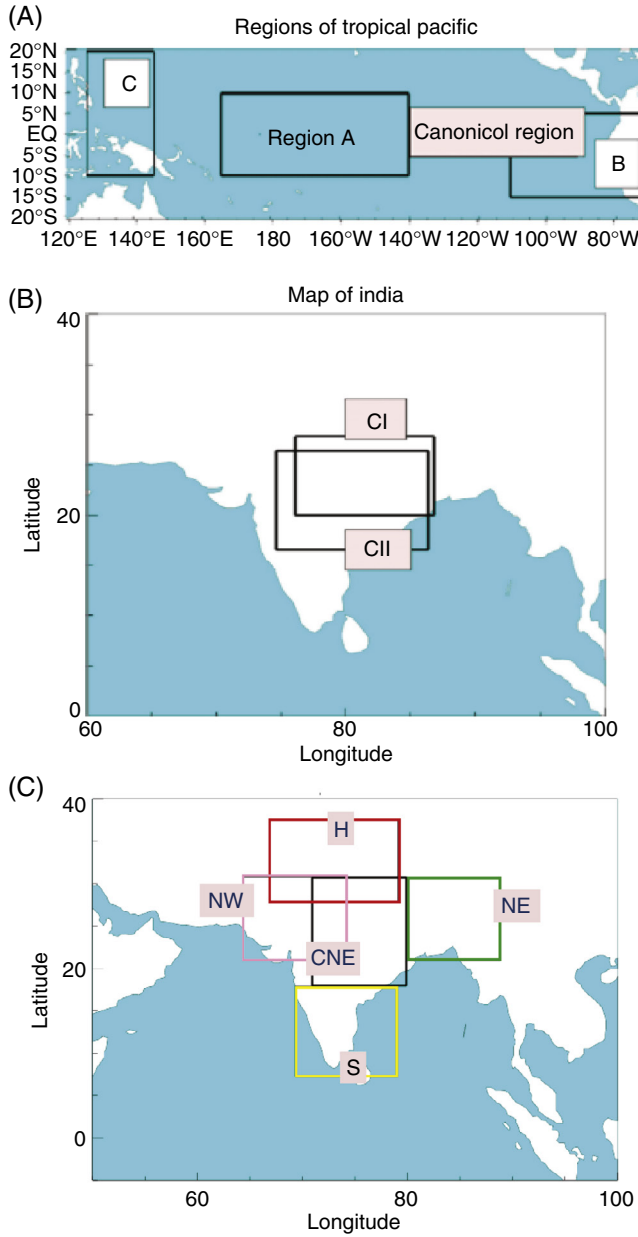

FIG. 11.6 Various regions used to explore ENSO–ISM regional teleconnection. Regions of the tropical Pacific used for defining different types of ENSO (A); map of India showing CI and CII region from CNE (B); map of India subdivided in five different arbitrary chosen regions—CNE, Hilly region (H), North West (NW), North East (NE), and Southern region (S) (C). "*CNE*, Central North East; *ENSO*, El Niño southern oscillation; *ISM*, Indian summer monsoon."

Years of ENSO phases were calculated following the definition of respective phases. Those were then subtracted from the average of the whole record to indicate the anomaly value of that parameter in the respective ENSO phases. For significant testing, the hypergeometric test (Meyer, 1997; Ropelewski and Halpert, 1987) is applied which is also used in other studies (Tedeschi et al., 2013; Grimm, 2004). Compositing is useful to better capture asymmetries in response to El Niño from La Niña phases.

Results showed that not all regions in India are affected by ENSO (Roy, 2017; Roy et al., 2017). So, two regional teleconnections were focused: (1) a positive rainfall signal around "hilly" and CNE region of India during La Niña (and vice versa for El Niño) and (2) a similar signal for regions of southern peninsular India (regions shown in Fig. 11.6C). Correlation study indicated that more than 50% of the CMIP5 models captured these two regional teleconnections, while the first signal is captured by more than 80% of models (Roy et al. 2017). Using compositing technique, it is found that most models again agree on the sign of regional teleconnection around the CNE and hilly region of India. That suggests the robustness of ENSO teleconnection in that region. Separating models based on High Top or Low Top did not make much difference. Even many CMIP6 models are unable to represent the regional summer rainfall patterns over India associated with ENSO (Mahendra et al. 2020).

Using CMIP5 model outputs in different ENSO phases, studies further investigated regional teleconnection in five arbitrarily chosen regions of the Indian subcontinent (Roy and Tedeschi, 2016), namely, CNE region, Hilly region (H), North West (NW), North East (NE), and Southern India (S) (Fig. 11.6C). To overcome issues of resolution in CMIP5 models, each region was kept at least 10 degrees wide, both longitude and latitude-wise. Local wind fields and remote influences from the tropical Pacific were considered and results were compared with observations/reanalysis to pinpoint areas of agreement and shortcomings. Meridional and zonal components of wind at 200 mb and 850 mb levels were explored.

Results among models and observations are more consistent for zonal velocity at 200 hPa (u-200) in CNE region (Fig. 11.7). It is also true for CI and CII regions (Roy et al. 2017). In CNE region, precipitation is generally negatively correlated with the local zonal eastward velocity at 200 hPa (u-200) in CMIP5 models and observation (Fig. 11.7). For La Niña, more precipitation, in general, is seen for almost all models, though less for El Niño. Moreover, during El Niño, u-200 is positive in almost all cases, while for La Niña it is negative which indicates a change in the direction of Walker circulation. However, analyses with meridional component of wind (v) at 200 mb (v-200) indicate circulation of the upper branch of Hadley cells in regions CNE and Southern India, though suggest the best agreement among models in comparison with other fields, but there are some deviations from observations, indicating missing mechanisms in models.

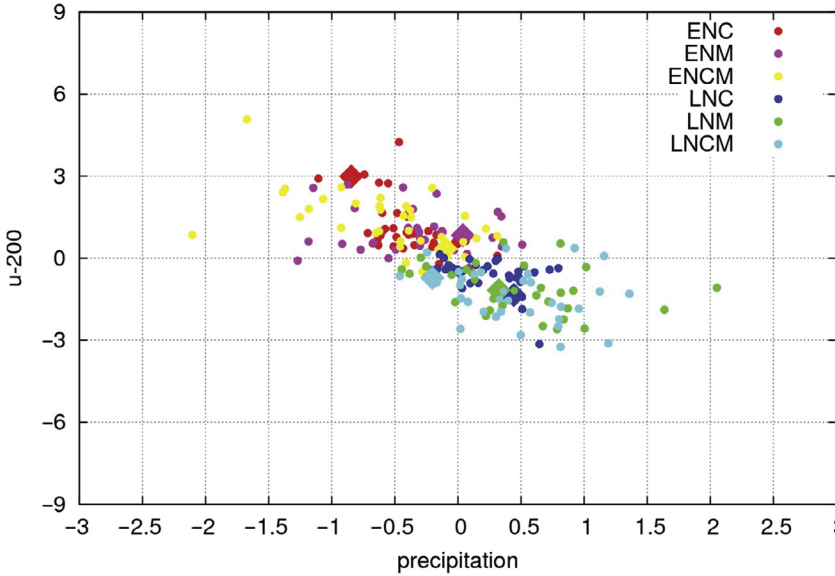

FIG. 11.7 Composite anomaly (JJA) plot around CNE region (18°N–31°N, 86°E–75°E) for ISM precipitation (mm/day) versus local zonal eastward velocity at 200 hPa (u-200) (m/s) in different phases of El Niño and La Niña in CMIP5 models. Composites for ENC, ENM, and ENCM are shown by red, pink ,and yellow, whereas that of LNC, LNM, and LNCM are shown by blue, green, and cyan, respectively. Data of observation/reanalyses are shown by the same colored large diamond. If models are in agreement with observations, then those diamonds are masked in the schematics. Results are similar if either CI or CII regions are used instead of CNE region (Roy and Tedeschi, 2016). "*ENC*, Canonical El Niño; *ENCM*, Canonical and Modoki El Niño; *ENM*, El Niño Modoki; *ISM*, Indian summer monsoon; *LNC*, *Canonical La Niña*; *LNCM*, Canonical and Modoki La Niña; *LNM*, La Niña Modoki."

Fig. 11.8 shows composite anomaly plot (JJA) for model ensemble mean in nine selected models (models shown in Fig. 11.4) for ISM (top) and SST (bottom) in different El Niño and La Niña cases. Results are also similar using all CMIP5 models. Significant regions at 95% level are outlined. Around CNE, there is less rain for all EN phases, while more rain for LN. Moreover, for SST there is warming around tropical Pacific for all EN cases while cooling for LN phases. Thus, there is a clear connection (anticorrelation) between tropical Pacific SST and ISM around CNE region of India in various ENSO phases (Fig. 11.8) (Roy et al. 2017). It is also consistent with the direction of the wind in Walker circulation (Fig. 11.7) and matches with observation too.

11.2.5 ISM in various ENSO phases: historical vs RCP scenario

Teleconnections between ISM and ENSO in CMIP5 simulations were explored by comparing historical period with future scenario (Roy et al. 2019). The

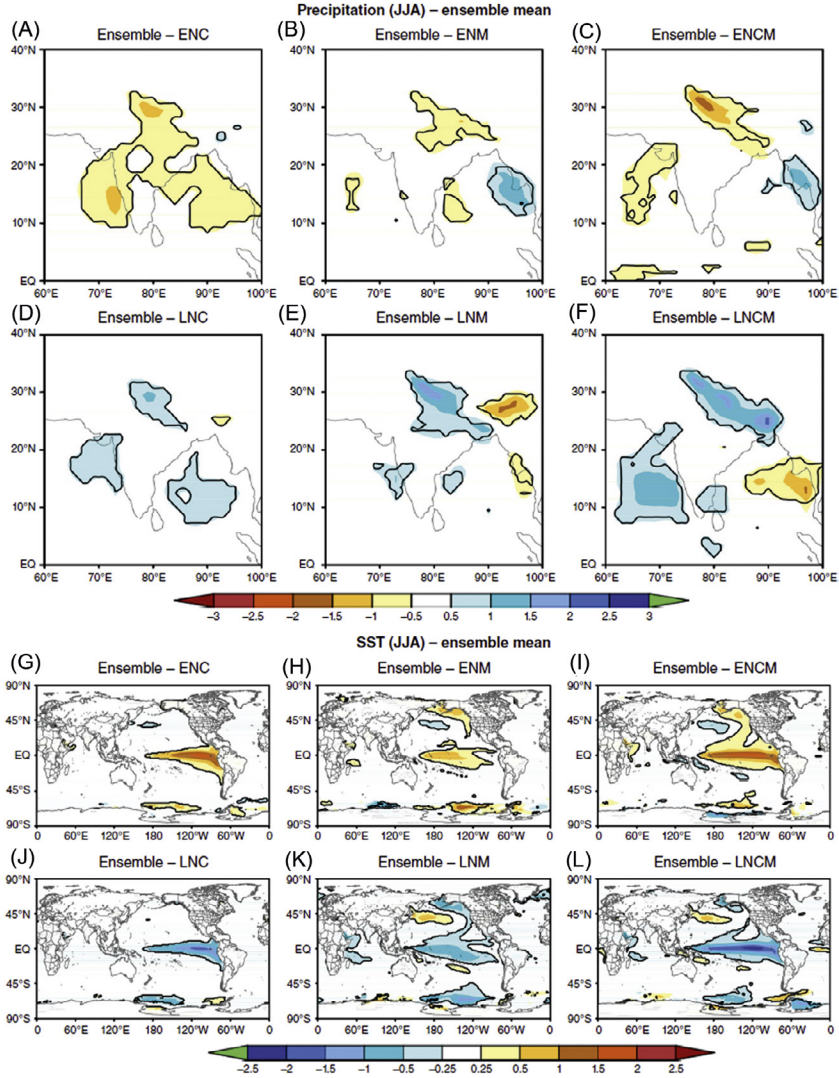

FIG. 11.8 Composite anomaly plot (JJA) for model ensemble mean in nine selected models of ISM precipitation (mm/day) (top, A–F) and SST (°C) (bottom, G–L). Composites are shown in different El Niño (A–C, G–I) and La Niña cases (D–F, J–L) (Roy et al., 2017). "*ISM*, Indian summer monsoon; *SST*, sea surface temperature."

correlation coefficients in the RCP and historical scenario between tropical Pacific SST and ISM are shown in two regions of CNE, namely, CI and CII (Fig. 11.9).

Almost all models show a negative correlation for the RCP as well as historical scenarios. Clustering around the one-to-one line is clearly noticed.

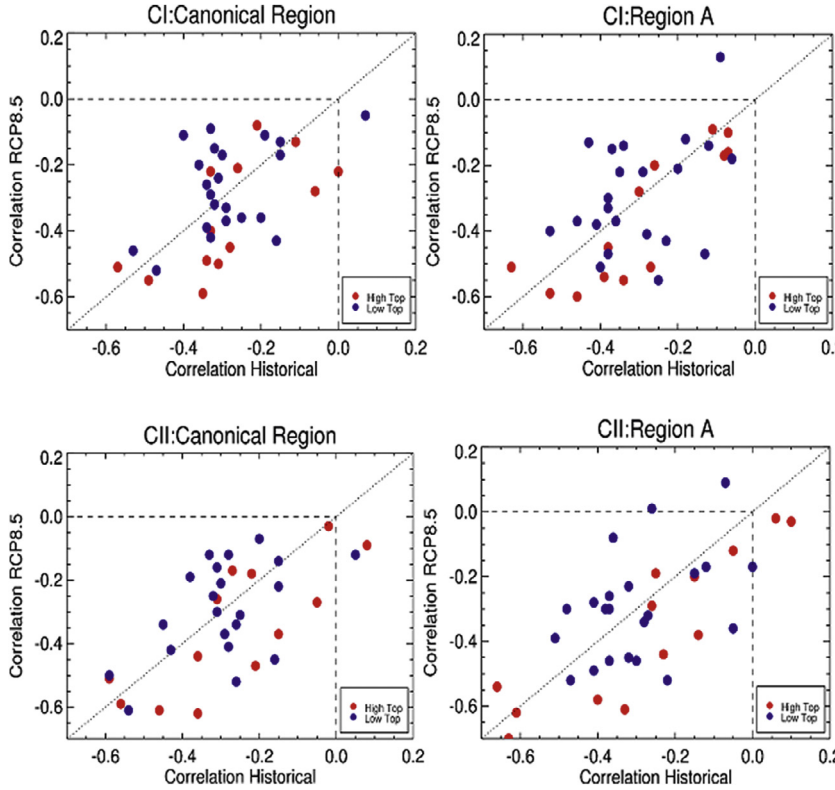

FIG. 11.9 Correlation between SST and ISM during RCP8.5 versus historical scenario. In the right, SST is chosen in region (A), whereas in the left canonical region is chosen. ISM rainfall is considered in two different regions of CNE, CI (top) and CII (bottom). In both scenarios, if model results show a negative correlation those are confined in a box of dashed lines (Roy et al., 2019). "*CNE*, Central North East*; ISM*, Indian summer monsoon; *SST*, sea surface temperature."

A tighter relationship, with lesser spread among models, is apparent when instead of SST of region A, the canonical region is used and also for CI instead of CII, respectively. These correlations are relatively insensitive to the choice of SST indices, (either Niño4 and Niño3 instead of region A and canonical region, respectively). High Top or Low Top models do not make many differences.

A subset of models was selected, based on their ability to simulate the spatial pattern of ISM in the historical period (Jourdain et al. 2013, also shown in Fig.11.4), and those are used in the CNE region, to examine future predictions (Fig. 11.10). Results were also similar using all models. For mixed canonical Modoki events and pure canonical ENSO events, the teleconnection is spatially extended in the future over most of India. Interestingly for pure ENSO Modoki events, that teleconnection disappears, and practically no influence is

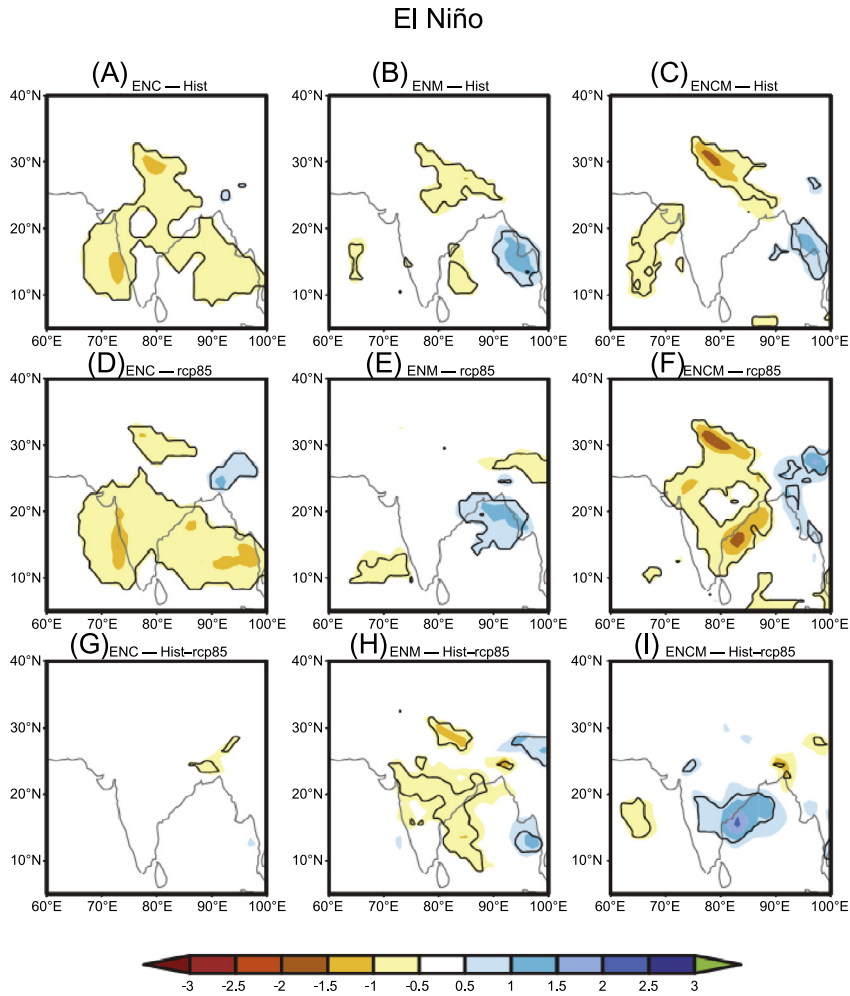

FIG. 11.10 Composite anomaly plot (JJA) for model ensemble mean in selected models of ISM (mm/day) for El Niño and La Niña cases. ISM composites in historical (A–C), RCP8.5 (D–F) and historical-RCP8.5 scenarios (G–I) are shown. Results are similar combining all models. Ensemble mean for various ENSO phases are shown [ENC/ LNC (A, D, G), ENM/ LNM (B, E, H) and ENCM/LNCM (C, F, I)]. Significant regions are marked by a black outline (Roy et al., 2019). "*ENC*, Canonical El Niño; *ENCM*, Canonical and Modoki El Niño; *ENM*, El Niño Modoki; *ENSO*, El Niño southern oscillation; *ISM*, Indian summer monsoon; *LNC*, Canonical La Niña; *LNCM*, Canonical and Modoki La Niña; *LNM*, La Niña Modoki."

detected in the future in any parts of India (Fig. 11.10). A rainfall decomposition technique revealed a battle between changes in moisture change which act to strengthen the rainfall teleconnection and changes in circulation which act to weaken it (Roy et al. 2019).

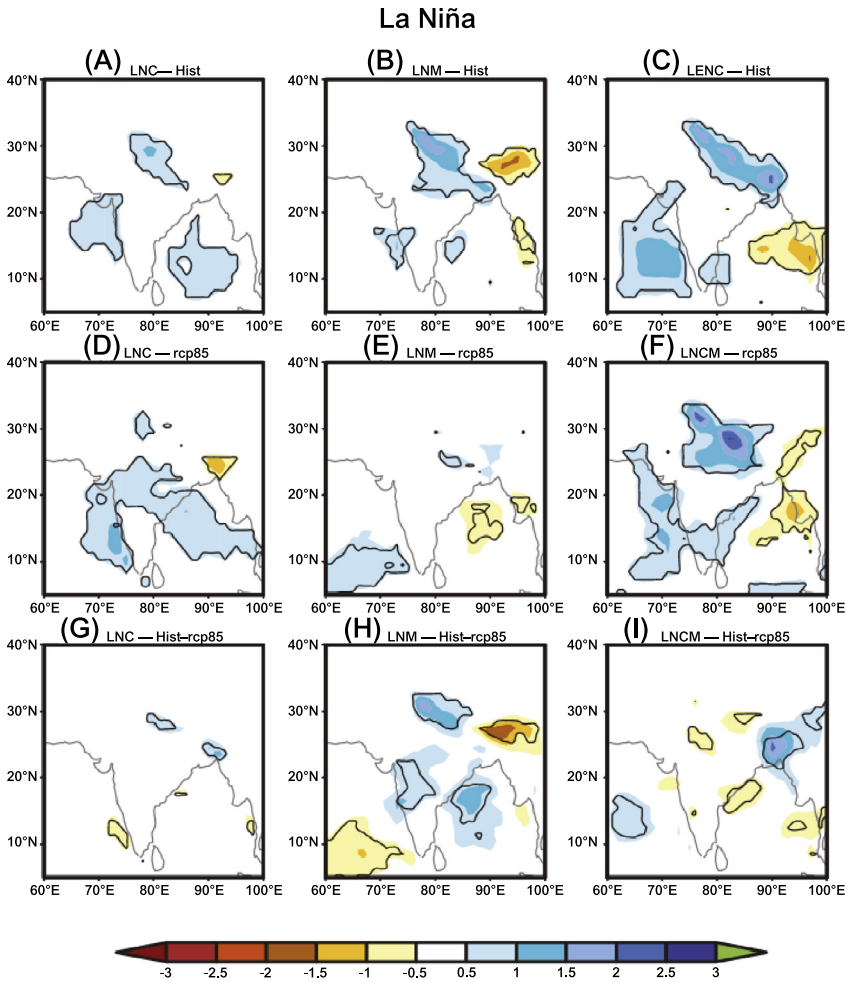

FIG. 11.10 (continued)

11.3 Mechanisms: role of natural factors

Studies addressed on mechanisms and discussed the importance on an improved understanding of the tropic and mid-latitude connection (Prabhu et al., 2016; Roy and Kripalani, 2019a; Roy, 2018b). Moreover, Roy and Kripalani (2019a) analyzed the role of natural factors, mainly the sun on ISM in a holistic way by exploring various major tropospheric and stratospheric modes. Initiated by solar decadal variability it depicted coupling in the ocean–atmosphere system, by formulating a flow chart, that involved ENSO (Fig. 11.11). Possible mechanisms for ENSO Modoki (or CP ENSO),

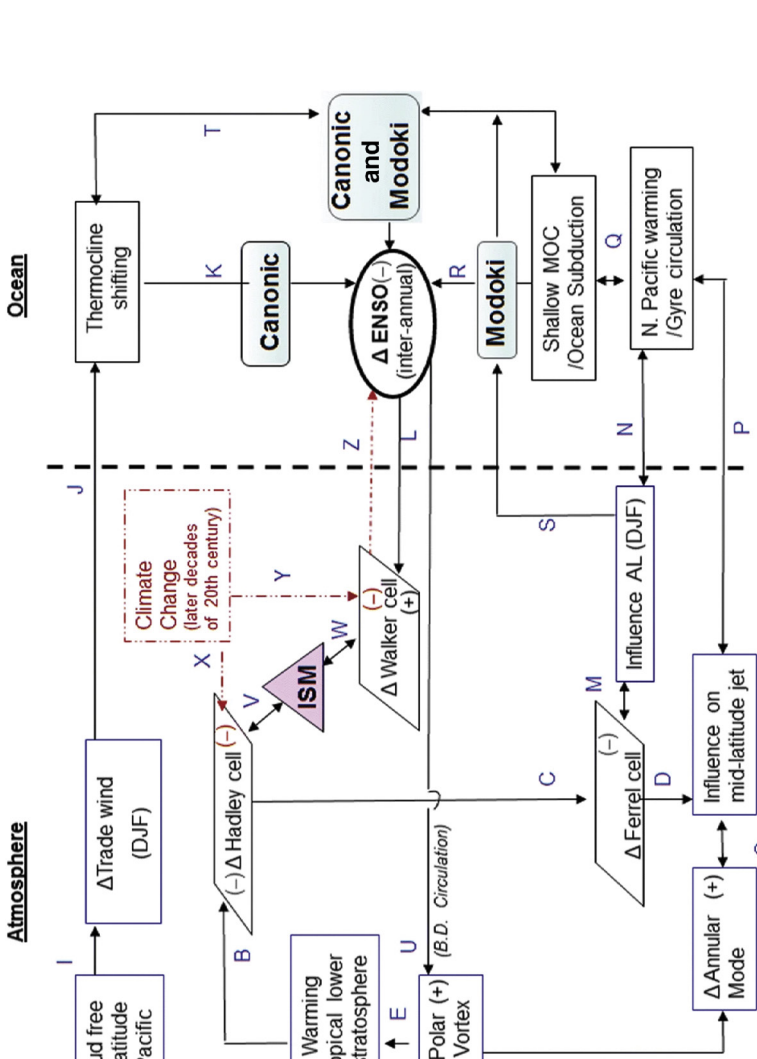

FIG. 11.11 A flow chart is presented depicting the role of the sun in atmosphere and ocean coupling mainly during DJF. Possible mechanisms for ENSO Modoki, Canonic ENSO, and Canonic–Modoki ENSO are suggested. Three major variability, namely, solar, QBO, and ENSO are shown by oval outlines, whereas major circulations, responsible for modulating the effect are shown by nonrectangular parallelograms. Pathways of signals are marked by "A" – "Z," e.g., Brewer Dobson (B.D.) circulation via ENSO can influence Polar vortex is shown by "U." *Dash-dotted lines* indicate how ENSO-related teleconnection (e.g., ISM) can be altered in the latter decades of the last century. Directions of change in behavior are shown by "+" (for increase) or "–" (for decrease) (Roy and Kripalani, 2019a). *DJF*, December-January-February; *ENSO*, El Niño southern oscillation; *ISM*, Indian summer monsoon.

Canonic (or EP) ENSO, and Canonic–Modoki (EP and CP) ENSO were proposed considering their relevance to the decadal-scale variation of mid-latitude jets, Hadley and Walker circulation. The upper stratospheric polar vortex features were included too. Some results of solar signature were presented which could possibly trigger different types of ENSO, agreeing with proposed pathways of the flow chart. Since the 1970s, there was a changing behavior of the ENSO (Ashok and Yamagata, 2009; Yeh et al., 2009), which was also addressed.

Mechanisms of ENSO–ISM teleconnection and a change in the later period were addressed even in many earlier studies (Kripalani and Kulkarni, 1997; Krishna Kumar et al., 1999, etc). ENSO–ISM relationship had significant changes in the past three multidecadal epochs (early: 1931–1960, middle: 1961–1990, and recent: 1991–2015) (Seetha et al., 2020). The rainfall during the early epoch was above normal, whereas in the last two, it was relatively dry. The ISMR–ENSO connection and its deviation are more distinct in CNE India. During the early epoch, the effect of La Niña was more dominant which can be attributed to the excess rainfall, whereas the ISM during the consecutive two multidecadal epochs is below normal and may be attributed to the strong El Niño events. The changes in equatorial Walker and regional Hadley circulations during the three epochs are linked to the changes in rainfall and other circulation-related parameters (Seetha et al. 2020).

Some studies further focused later two decades of the last century where CP ENSO became more persistent and frequent (Ashok and Yamagata, 2009; Yeh et al. 2009) and disruption in ISM–ENSO connection was more pronounced (Roy, 2018b; Roy and Kripalani, 2019b; Kumar et al. 1999). There was also a common shifting point for regional monsoon–ENSO relationship around the 1970s with a recovery in the late 1990s (Yim et al., 2013). Roy (2018b) separated out a period 1976–1996 that covered two full solar cycles, where two explosive volcanos erupted during active phases of strong solar cycles. The similar period also matched the period of abrupt global warming. A hypothesized mechanism was proposed that could be generated by explosive volcanos and initiated via a preferential alignment of the NAO phase (Fig. 11.12). Inciting extratropical Rossby wave to modulate the Aleutian Low (AL) had an influence on CP ENSO. The usual effect of East-West (E-W) Walker circulation on ISM was partly overtaken by North-South (N-S) Hadley circulation. Winter NAO and Eurasian snow played an important role to modulate N-S Hadley circulation (see Chapter 12). Disruption of ENSO and ISM teleconnection during that period of abrupt warming and a subsequent recovery thereafter can be explained from that angle. Interestingly, the ensemble of CMIP5 model, and also individual models, fails to conform with such observation. These issues were further elaborated by Roy and Kripalani (2019b). Observation suggested that the regional Hadley circulation, via NAO in the northern hemisphere and IOD in the southern hemisphere, had roles in the change in ISM behavior (Roy and Collins, 2015). More recently, importance of western north Pacific low-level circulation influence on modulating

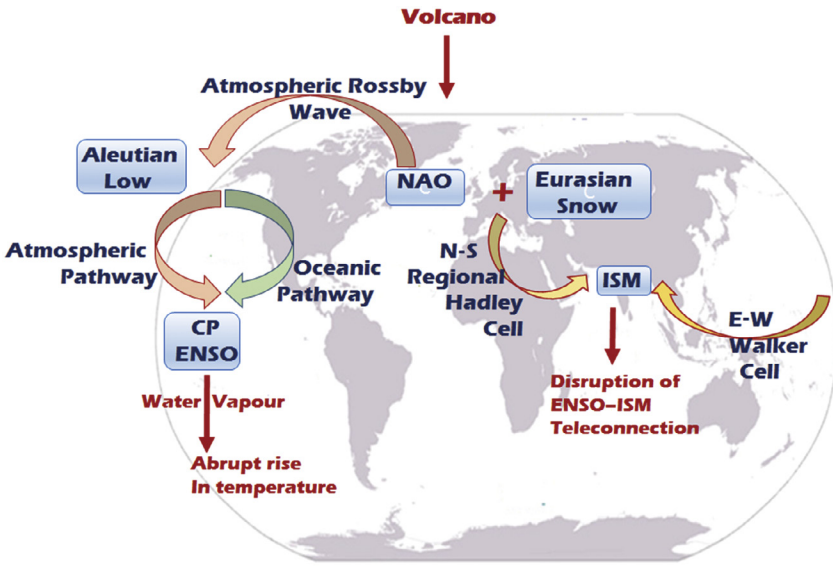

FIG. 11.12 A proposed schematic of hypothesized mechanisms for a change in ISM–ENSO teleconnection during 1976–1996 is presented. It is initiated by explosive volcanos, those erupted during active phases of strong solar cycles. That influences various places [Aleutian Low (AL) and Eurasian snow cover] and modulates various modes (ISM, NAO, and CP ENSO), shown by the blue box. From North Atlantic, AL is impacted via atmospheric Rossby waves. That signal is transported to trigger CP ENSO through Oceanic (*green arrow*) and atmospheric pathways (*pink arrow*). Increased CP ENSO raises atmospheric water vapor and can cause an abrupt rise in global temperature (the effect is shown by red). Combination of Eurasian Snow and NAO strongly modulates N-S regional Hadley circulation (*yellow arrow*) to impact ISM. A disruption in usual ENSO–ISM teleconnection is thus seen (shown by red) which normally occurs via E-W Walker circulation (*yellow arrow*) (Roy, 2018b). "*CP ENSO*, Central Pacific ENSO; *ISM*, Indian summer monsoon; *NAO*, North Atlantic oscillation."

ENSO–ISM teleconnections is highlighted (Mahendra et al., 2020; Ramu et al., 2020). Such features though well captured in the observation but shown missing in models (Roy and Kripalani, 2019b). Analyses on global hydrological cycle suggest that the differences among models mainly originate in regional levels and could be related to inconsistency in representing regional teleconnection features. Interestingly, in terms of global thermodynamic scaling arguments, all models perform reasonably well (Roy and Kripalani, 2019b).

11.4 Discussion and summary

The variability of ISM has major impacts on the socioeconomic structure of the country and this study focuses on the main factors that cause such variability. Teleconnection between ISM with two dominant tropical SST modes, namely, the ENSO and IOD are the key focus here. Results are presented and discussed using observed/ reanalyses data and CMIP5 simulations in historical as well as

future scenarios. Climatology and some features of ISM though captured well in some CMIP5 models, but there are large disagreements among models in various ISM-related features. Time series of ISM in future scenarios indicate that there is much larger uncertainty, compared to the rainfall of the whole world.

ENSO and IOD exert an offsetting impact on ISM, with El Niño tend to lower ISM rainfall, whereas a positive IOD tends to increase that. There is a positive skewness of the IOD where positive events tend to be stronger in amplitude than negative events. Moreover, the ENSO–IOD connection is positive and significant since the latter decades of the last century and it may correspond with either weak (strong) monsoon–ENSO relationship or strong (weak) monsoon–IOD relationship. The period when ISM–ENSO teleconnection weakened the teleconnection between ISM–IOD strengthened. Model results suggested that seasonal phase-locking of IOD is simulated well though models have limitations to account for the role of internal climate variability. If a model simulates a weak/strong ENSO, it is shown to generate a weak/strong IOD too. Due to an overly strong control by ENSO, the majority of CMIP5 models simulate an unrealistic IOD–ISMR correlation. In the simulated present-day scenario, a positive IOD is associated with a reduction in ISM rainfall. Such unrealistic correlation of the historical period is relevant to the future projection of ISM and will cause an underestimation/overestimation in the projected rainfall. Uncertainties in the projection of ISM can partly be induced by present-day simulation of ENSO, IOD, their connection, and their correlations with ISM.

For ENSO and ISM teleconnection, especially three different categories, i.e., Canonical, Modoki, and mixed Canonical, and Modoki cases are focused. Correlation and compositing technique both indicated that CMIP5 models capture regional teleconnections in CNE well in models as in observations. Even 80% of models agree on the sign of regional teleconnection around the CNE, suggesting the robustness of ENSO teleconnection in that region. In the CNE region, precipitation is generally negatively correlated with the local zonal eastward velocity at 200 hPa (u-200) in CMIP5 models and matches with observation. However, for the meridional velocity at 200 hPa (v-200), models though suggest highly consistent behavior but deviates from observation. In the historical period for all ENSO subcategories, there is a clear connection between the Walker circulation, tropical Pacific SST, and ISM rainfall around the CNE India in CMIP5 models and observation/reanalyses.

Using a subset of selective models, ISM and the ENSO teleconnection were further analyzed for a future scenario and compared with historical cases in various ENSO events. Interestingly, for future cases, the situation changes. For mixed canonical Modoki events and pure canonical ENSO events, that teleconnection from regions of CNE India is spatially extended over most of India in the future, though disappears for pure ENSO Modoki events. Practically no influence is detected in future for pure Modoki cases in any part of India. However, in terms of ISM–ENSO teleconnection, when the focus is only on tropical Pacific SST, almost all models show a negative correlation in regions

of CNE India (CI and CII) not only for historical scenarios but also for future cases. These correlations are relatively insensitive to the choice of various SST indices (either Niño4 and Niño3 instead of SST of region A and canonical region, respectively). Lesser spread among models is apparent when SST of the canonical region is used instead of region A and also if CI from CNE India is considered instead of CII. A rainfall decomposition technique revealed a battle between changes in moisture which acts to strengthen the rainfall teleconnection and changes in circulation which acts to weaken it.

Focusing on mechanisms, tropic, mid-latitude connection, and the role of natural factors were addressed. Formulating a flow chart, coupling in the atmosphere and ocean is presented, which is initiated by solar decadal-scale variability and involved different types of ENSO. Considering relevance to the decadal-scale variation of Hadley, Walker circulation and mid-latitude jets, possible mechanisms for ENSO Modoki (or CP ENSO), Canonical (or EP) ENSO, and Canonical–Modoki (or CP and EP) ENSO were proposed. Finally, disruption of ISM–ENSO teleconnection in the latter two decades of the 20th century is addressed. One hypothesized mechanism is proposed that could be originated in the North Atlantic and modulates regional Hadley circulation, which partly overtakes influence from the Walker circulation on ISM.

Overall, this study analyzed results of observation and models to improve our understanding of the interaction between some important tropical SST modes and ISM. It would be useful to advance future prediction skills of ISM rainfall and reduce uncertainty in models.

Conflict of Interest

There is no conflict of interest.

Funding

This work did not receive any funding.

Acronyms

AL	Aleutian Low.
CESM-LE	Community Earth System Model Large Ensemble.
CMIP5	Coupled Model Inter-comparison Project Phase 5.
CNE	Central North East.
CP ENSO	Central Pacific ENSO.
DJF	December-January-February.
E-W	East West.
EP ENSO	East Pacific ENSO.
ENC	Canonical El Niño.
ENCM	Canonical and Modoki El Niño.
ENM	El Niño Modoki.
ENSO	El Niño Southern Oscillation.

H	High Top.
IO	Indian Ocean.
IOD	Indian Ocean Dipole.
ISM	Indian Summer Monsoon.
ISMR	Indian Summer Monsoon Rainfall.
JJA	June-July-August.
L	Low Top.
LNC	Canonical La Niña.
LNCM	Canonical and Modoki La Niña.
LNM	La Niña Modoki.
MMEM	Multi-Model Ensemble Mean.
MOC	Meridional Overturning Circulation.
NAO	North Atlantic Oscillation.
N-S	North-South.
RCP	Representative Concentration Pathway.
SON	September-October-November.
SST	Sea Surface Temperature.

References

Ashok, K., Guan, Z., Yamagata, T., 2001. Impact of Indian Ocean dipole on the relationship between the Indian monsoon rainfall and ENSO. Geophys. Res. Lett. 28 (23), 4499–4502.

Ashok, K., Guan, Z., Saji, N.H., Yamagata, T., 2004. Individual and combined influences of ENSO and the Indian Ocean Dipole on the Indian summer monsoon. J. Clim. 17, 3141–3155.

Ashok, K., Behera, S.K., Rao, S.A., Weng, H., Yamagata, T., 2007. El Niño Modoki and its possible teleconnection. J. Geophys. Res. 112, C11007. doi:10.1029/2006JC003798.

Ashok, K., Yamagata, T, 2009. Climate change the El Niño with a difference. Nature 461, 481–484. doi:10.1038/461481a.

Azad, S., Rajeevan, M., 2016. Possible shift in the ENSO-Indian monsoon rainfall relationship under future global warming. Sci. Rep. 6, 20145.

Behera, S.K., Luo, J.J., Masson, S., Rao, S.A., Sakuma, H., 2006. A GCM study on the interaction between IOD and ENSO. J. Clim. 19, 1688–1705.

Bollasina, M.A., et al., 2011. Anthropogenic aerosols and the weakening of the South Asian summer monsoon. Science 502. doi:10.1126/science.1204994 334.

Brown, J.N., McIntosh, P.C., Pook, M.J., Risbey, J.S., 2009. An investigation of the links between ENSO flavors and rainfall processes in Southeastern Australia. Mon. Weather Rev. 137, 3786–3795.

Cai, W., Cowan, T., 2009. La Niña Modoki impacts Australia autumn rainfall variability. Geophys. Res. Lett. 36 L12805doi:2009GL037885.

Cai, W., Qiu, Y., 2012. An observation-based assessment of nonlinear feedback processes associated with the Indian Ocean Dipole. J. Clim. 26, 2880–2890.

Cai, et al., 2015. ENSO and greenhouse warming. Nat. Clim. Change 5, 849–859.

Cappondonti, A., et al., 2015. Understanding ENSO diversity. Bull. Am. Meteor. Soc. 96, 921–938. doi:10.1175/BAMS-D-13-00117.1.

Chakravorty, S., Chowdary, J.S., Gnanaseelan, C., 2013. Spring asymmetric mode in the tropical Indian Ocean: role of El Nino and IOD. Clim. Dyn. 40, 1467–1481. doi:10.1007/s00382-012-1340-1.

Charlton-Perez, A.J., 2013. On the lack of stratospheric dynamical variability in low-top versions of the CMIP5 models. J. Geophys. Res. Atmos. 118 (6). doi:10.1002/jgrd.50125.

Cherchi, A., Navarra, A., 2013. Influence of ENSO and of the Indian Ocean Dipole on the Indian summer monsoon variability. Clim. Dyn. 41, 81–103 https://doi.org/10.1007/s00382-012-1602-y.

Chou, C., Neelin, J., Chen, C., Tu, J., 2009. Evaluating the "rich-get-richer" mechanism in tropical precipitation change under global warming. J. Clim. 22, 1982–2005.

Chung, C.T.Y., Power, S.B., Arblaster, J.M., Rashid, H.A., Roff, G.L., 2014. Nonlinear precipitation response to El Niño and global warming in the Indo-Pacific. Clim. Dyn. 42, 1837–1856. doi:10.1007/s00382-013-1892-8.

Gill, A.E., 1980. Some simple solutions of heat induced tropical circulations. Q. J. R. Meteorol. Soc 106, 447–462.

Goswami, B.N., Venugopal, V., Sengupta, D., Madhusoodanan, M.S., Xavier, P.K., 2006. Increasing trend of extreme rain events over india in a warming environment. Science 314, 1442.

Grimm, A.M., 2004. How do La Niña events disturb the summer monsoon system in Brazil? Clim. Dyn. 22, 123–138.

Held, I.M., Soden, B.J., 2006. Robust responses of the hydrological cycle to global warming. J. Clim. 19, 5686.

Hrudya, P.H., Varikoden, H., Vishnu, R., et al., 2020a. Changes in ENSO-monsoon relations from early to recent decades during onset, peak and withdrawal phases of Indian summer monsoon. Clim. Dyn. 55, 1457–1471. doi:10.1007/s00382-020-05335-x.

Hrudya, P.H., Varikoden, H., Vishnu, R., 2020b. A review on the Indian summer monsoon rainfall, variability and its association with ENSO and IOD. Meteorol. Atmos. Phys. doi:10.1007/s00703-020-00734-5.

Huang, P., 2014. Regional response of annual-mean tropical rainfall to global warming. Atmos. Sci. Lett. 15, 103–109. doi:10.1002/asl2.475.

Huang, P., Xie, S.-P., 2015. Mechanisms of change in ENSO-induced tropical Pacific rainfall variability in a warming climate. Nat. Geosci. 8, 922–926. doi:10.1038/ngeo2571.

Hui, C., Zheng, X., 2018. Uncertainty in Indian Ocean Dipole response to global warming: the role of internal variability. Clim. Dyn. 51, 3597–3611. doi:10.1007/s00382-018-4098-2.

Hurwitz, M.M., et al., 2014. Extra-tropical atmospheric response to ENSO in the CMIP5 Models. Clim. Dyn. doi:10.1007/s00382-014-2110-z.

John, O., Allan, R.P., Soden, J., 2009. How robust are observed and simulated precipitation responses to tropical ocean warming? Geophys. Res. Lett. 36, L14702.

Jourdain, N.C., Sen Gupta, A., Taschetto, A.S., Ummenhofer, C.C., Moise, A.F., Ashok, K., 2013. The Indo-Australian monsoon and its relationship to ENSO and IOD in reanalysis data and the CMIP3/CMIP5 simulations. Clim. Dyn. 41, 3073–3102. doi:10.1007/s00382-013-1676-1.

Kao, H.-Y., Yu, J.-Y., 2009. Contrasting eastern-Pacific and central-Pacific types of El Nino. J. Clim. 22, 615–632.

Kripalani, R.H., Kulkarni, A., 1997. Climatic impact of EI Niño/La Niña on the Indian monsoon: a new perspective. Weather 52, 39–46.

Krishna Kumar, K., Rajagopalan, B., Cane, M.A., 1999. On the weakening relationship between the Indian monsoon and ENSO. Science 284, 2156–2159.

Krishnaswami, J., Vaidyanathan, S., Rajagopalan, B., Bonnel, M., Sankaran, M., Bhalla, R.S., et al., 2014. Non-stationary and non-linear influence of ENSO and Indian Ocean Dipole on Indian summer monsoon rainfall and extreme rain events. Clim. Dyn. doi:10.1007/s00382-014-2288-0.

Kug, J.-S., Jin, F.-F., An, S.-I., 2009. Two types of El Niño events: cold tongue El Niño and warm pool El Niño. J. Clim. 22, 1499–1515.

Krishna Kumar, K., Rajagopalan, B., Cane, M.A., 1999. On the weakening relationship between the Indian monsoon and ENSO 284 (5423), 2156–2159. doi:10.1126/science.284.5423.2156.

Kumar, K.K., Rajagopalan, B., Hoerling, M., Bates, G., Cane, M., 2006. Unraveling the mystery of Indian monsoon failure during El Niño. Science 314, 115–119.

Li, Z., Lin, X., Cai, W., 2017. Realism of modelled Indian summer monsoon correlation with the tropical Indo-Pacific affects projected monsoon changes. Sci. Rep. *7* (1), 4929. doi:10.1038/s41598-017-05225-z https://doi.org/.

Liu, L., et al., 2014. Indian Ocean variability in the CMIP5 multi-model ensemble: the zonal dipole mode. Clim. Dyn 43, 1715–1730.

Mahendra, N., Chowdary, J.S., Darshana, P., Sunitha, P., Parekh, A., Gnanaseelan, C., 2020. Interdecadal modulation of interannual ENSO-Indian Summer monsoon rainfall teleconnections in observations and CMIP6 models: regional patterns. Int. J. Climatol. doi:10.1002/joc.6973.

Meyer, P.L., 1970. Introductory Probability and Statistical Applications. Addison-Wesley, Boston, MA.

Ng, B., Cai, W., Cowan, T., et al., 2018. Influence of internal climate variability on Indian Ocean Dipole properties. Sci. Rep. 8, 13500. doi:10.1038/s41598-018-31842-3.

Ogata, T., Xie, S.-P., Lan, J., Zheng, X.-T., 2012. Importance of ocean dynamics for the skewness of the Indian Ocean Dipole Mode. J. Clim. 26, 2145–2159.

Osprey, S.M., Gray, L.J., Hardiman, S.C., Butchart, N., Hinton, T.J., 2013. Stratospheric variability in twentieth-century CMIP5 simulations of the met office climate model: high top versus low top. J. Clim. 26, 1595–1606.

Prabhu, A., Kripalani, R.H., Preethi, B., Pandithurai, G., 2016. Potential role of the February–March southern annular mode on the Indian summer monsoon rainfall: a new perspective. Clim. Dyn 47 (3), 1161–1179.

Preethi, B., Kripalani, R.H., Krishna Kumar, K., 2010. Indian summer monsoon rainfall variability in global coupled ocean-atmospheric models. Clim. Dyn. 35, 1521–1539.

Preethi, B., Sabin, T., Adedoyin, J., et al., 2015. Impacts of the ENSO Modoki and other tropical Indo-Pacific climate-drivers on African Rainfall. Sci. Rep. 5, 16653. doi:10.1038/srep16653.

Rajeevan, M., Unnikrishnan, C.K., Preethi, B., 2012. Evaluation of the ENSEMBLES multi-model seasonal forecasts of Indian summer monsoon variability. Clim. Dyn. 38, 2257–2274.

Ramu, D.A., Chowdary, J.S., Pillai, P.A., Sradhara, S.N.S., Koteswararao, K., Ramakrishna, S.S.V.S., 2020. Impact of El Niño Modoki on Indian summer monsoon rainfall: role of western north Pacific circulation in observations and CMIP5 models. Int. J. Climatol. 40, 2117–2133.

Rasmussen, E.M., Carpenter, T.H., 1983. The relationship between eastern equatorial Pacific SST and rainfall over India and Sri Lanka. Mon. Weather Rev. 111, 517–552.

Riahi, K., Rao, S., Krey, V., Cho, C., Chirkov, V., Fischer, G., et al., 2011. RCP-8.5—a scenario of comparatively high greenhouse gas emission. Clim. Change 109, 33–57. doi:10.1007/s10584-011-0149-y.

Ropelewski, C.F., Halpert, M.S., 1987. Global and regional scale precipitation patterns associated with the El Niño-Southern Oscillation. Mon. Weather Rev. 115, 1606–1626.

Roy, I., Collins, M., 2015. On Identifying the role of Solar variability and the El Niño Southern Oscillation on Indian summer monsoon rainfall. Atmos. Sci. Lett. 16 (2), 162–169. doi:10.1002/asl2.547.

Roy, I., Tedeschi, R.G., 2016. 'Influence of ENSO on regional ISM precipitation—local atmospheric Influences or remote influence from Pacific. Atmosphere 7, 25. doi:10.3390/atmos7020025.

Roy, I., Tedeschi, R.G., Collins, M., 2017. 'ENSO teleconnections to the Indian summer monsoon in observations and models. Int. J. Climatol. 37 (4), 1794–1813. doi:10.1002/joc.4811.

Roy, I., 2017. Indian summer monsoon and El Niño southern oscillation in CMIP5 models: a few areas of agreement and disagreement. Atmosphere 8 (8), 154. doi:10.3390/atmos8080154.

Roy, I., 2018. 'Climate Variability and Sunspot Activity—Analysis of the Solar Influence on Climate'. Springer Nature 18 chapters, 216 pages, ISBN 978-3-319-77107-6, doi:10.1007/978-3-319-77107-6.

Roy, I, 2018b. Addressing on abrupt global warming, warming trend slowdown and related features in recent decades. Front. Earth Sci. 6, 136. doi:10.3389/feart.2018.00136.

Roy, I., Gagnon, A.S., Siingh, D., 2018. 'Evaluating ENSO teleconnections using observations and CMIP5 models. Theor. Appl. Climatol. doi:10.1007/s00704-018-2536-z 2018.

Roy, I., Kripalani, R., 2019a. 'The role of natural factors (Part 1): addressing on mechanism of different types of ENSO, related teleconnections and solar influence'. Theor. Appl. Climatol., 1–12. doi:10.1007/s00704-018-2597-z.

Roy, I., Kripalani, R., 2019b. The role of natural factors (Part 2): Indian summer monsoon in climate change period—Observation and CMIP5 models. Theor. Appl. Climatol. doi:10.1007/s00704-019-02864-2.

Roy, I., Tedeschi, R.G., Collins, M., 2019. ENSO teleconnections to the Indian summer monsoon under changing climate. Int. J. Climatol. doi:10.1002/joc.5999.

Roy, I., 2020. Major climate variability and natural factors in boreal winter. Pure Appl. Geophys. doi:10.1007/s00024-020-02522-z.

Saji, N.H., Goswami, B.N., Vinayachandran, P.N., Yamagata, T., 1999. A dipole mode in the tropical Indian Ocean. Nature 401, 360–363.

Saji, N.H., Yamagata, T., 2003. Possible impacts of Indian Ocean dipole mode events on global climate. Clim. Res. 25, 151–169.

Seager, R., Naik, N., Vecchi, G.A., 2010. Thermodynamic and dynamic mechanisms for large-scale changes in the hydrological cycle in response to global warming. J. Clim. 23, 4651–4668. doi:10.1175/2010JCLI3655.1.

Seager, R., Naik, N., Vogel, L., 2012. Does global warming cause intensified interannual hydroclimate variability? J. Clim 25, 3355–3372. doi:10.1175/JCLI-D-11-00363.1.

Seetha, C.J., et al., 2020. Significant changes in the ENSO-monsoon relationship and associated circulation features on multidecadal timescale. Clim. Dyn. 54, 1491–1506.

Seviour, W.J.M., Gray, L.J., Mitchell, D.M, 2016. Stratospheric polar vortex splits and displacements in the high-top CMIP5 climate models. J. Geophys. Res.: Atmos. 121 (4), 1400–1413.

Sikka, D.R., 1980. Some aspects of large-scale fluctuations of summer monsoon rainfall over India in relation to fluctuations in the planetary and regional scale circulation parameters. Proc. Indian Acad. Sci. (Earth Planet Sci.) 89, 179–195.

Taylor, K.E., Stouffer, R.J., Meehl, G.A., 2012. An overview of CMIP5 and the experimental design. Bull. Am. Meteor. Soc. 93, 485–498. doi:10.1175/BAMS-D-11-00094.1.

Tedeschi, R.G., Cavalcanti, I.F.A., Grimm, A.M., 2013. Influences of two types of ENSO on South American precipitation. Int. J. Climatol. 33, 1382–1400. doi:10.1002/joc.3519.

Tedeschi, R.G., Collins, M., 2016. The influence of ENSO on South American precipitation during austral summer and autumn in observations and models. Int. J. Climatol. 36 (2), 618–635.

Ummenhofer, C.C., et al., 2009. What causes southeast Australia's worst droughts? Geophys. Res. Lett. 36, L04706.

Vibhute, A., Halder, S., Singh, P., Parekh, A., Chowdary, J.S., Gnanaseelan, C., 2020. Decadal variability of tropical Indian Ocean sea surface temperature and its impact on the Indian summer monsoon. Theor. Appl. Climatol. 141, 551–566. doi:10.1007/s00704-020-03216-1.

Wang, C., Fiedler, P.C., 2006. ENSO variability and the eastern tropical Pacific: a review. Progr. Oceanogr. 69, 239–266 2006.

Wang, B., Liu, J., Kim, H.J., Webster, P.J., Yim, S.Y., Xiang, B.Q., 2013. Northern Hemisphere summer monsoon intensified by mega-El Niño/southern oscillation and Atlantic multidecadal oscillation. Proc. Natl. Acad. Sci. USA 14, 5347–5352.

Webster, P.J., Moore, A.M., Loschnigg, J.P., Lebel, R.R., 1999. Coupled oceanic-atmospheric dynamics in the Indian Ocean during 1997–1998. Nature 401, 356–360.

Wu, Z., Zhang, P., 2015. Interdecadal variability of the mega-ENSO–NAO synchronization in winter. Clim. Dyn 45, 1117–1128.

Yeh, S., Kug, J., Dewitte, B., Kwon, M., Kirtman, B., Jin, F, 2009. El Niño in a changing climate. Nature 461, 511–514. doi:10.1038/nature08316.

Yim, S.Y., Wang, B., Liu, J., Wu, Z., 2013. A comparison of regional monsoon variability using monsoon indices. Clim. Dyn. 43, 1423–1437.

Yu, J.-Y., Kim, S.T., 2011. Relationships between extratropical sea level pressure variations and the Central-Pacific and Eastern-Pacific types of ENSO. J. Clim. 24, 708–720.

Yuan, Y., Yin, L.C., 2008. Decadal variability of the IOD-ENSO relationship. Chin. Sci. Bull. 53, 1745–1752.

Zhang, L., Wu, Z., Zhou, Y., 2016. Different impacts of typical and atypical ENSO on the Indian summer rainfall: ENSO-developing phase. Atmos.-Ocean 54, 440–456.

Zhang, P., Z., Wu, H., Chen, (2017). Interdecadal variability of the ENSO–North Pacific atmospheric circulation in winter. Atmos.-Ocean, 55, 110–120. doi: 10.1080/07055900.2017.1291411.

Zou, L., Zhou, T., 2015. Asian summer monsoon onset in simulations and CMIP5 projections using four Chinese climate models. Adv. Atmos. Sci. 32, 794. doi:10.1007/s00376-014-4053-z.